Sensors and Materials, Vol. 37, No. 7 (2025) 3285–3299
MYU Tokyo

S & M 4118

Computer-vision-based Displacement Monitoring System for Long-distance and Long-term Measurement on a Slope

I-Hui Chen* and Rui-Jia Yang

Department of Civil Engineering, National Chung Hsing University,
No. 145 Xingda Rd., South Dist., Taichung City 402, Taiwan

(Received March 12, 2025; accepted June 17, 2025)

Keywords: computer vision, AIoT, slope monitoring, ground movements

In this study, we present an innovative computer-vision-based displacement monitoring (CVDM) instrument, which includes a microcomputer, camera module, telescopic lens, and chessboard. The computer vision technology is employed to detect ground movements with an ultralong-distance, long-term, solar-powered, and real-time monitoring system. The average standard deviations and resolutions of three-axis displacements in the CVDM are 0.06 pixels and 0.01 cm at the 30 cm distance and 0.95 pixels and 0.10 cm at the 50 m distance, respectively, in experimental tests. The CVDM system can reach an ultralong distance of 1000 m in the field. The standard deviation and resolution of the ultralong-distance test are 0.33 pixels and 0.27 cm, respectively. Then, the CVDM system was installed inside a self-designed enclosure for long-term and real-time monitoring on a slope of the Jiufenershan landslide area with a 33 m distance between the enclosure and a chessboard. The CVDM system in the area can detect four frames of image recognition per second and transmit three-axis relative displacement and image data every 10 min with a 5G network for 24-h monitoring. Finally, the CVDM system is the artificial intelligence of things (AIoT) solution for computer-vision-based, economically efficient, and energy-saving slope monitoring.

1. Introduction

There is a need for the real-time, long-term, and early-warning monitoring of slope movement in landslide areas. Handy and automated monitoring devices are necessary for outlying mountainous areas, because usually, manpower and electric power are insufficient.(1) When landslides occur in mountain villages, a real-time and reliable monitoring system is needed for emergency response. In this study, we developed a noncontact image recognition instrument with a microcomputer, camera, and chessboard to monitor the displacement of engineering structures or landslide slopes to provide 24 h monitoring data and image information. Traditionally, the Global Positioning System or theodolites are often used for long-distance measurements.(2) However, these instruments are expensive and energy-consuming. Other conventional displacement monitoring sensors commonly employed in civil engineering

*Corresponding author: e-mail: cih82ian@nchu.edu.tw
https://doi.org/10.18494/SAM5615

ISSN 0914-4935

applications, such as extensometers and inclinometers, remain relatively costly and are not easily adaptable for monitoring internal structural deformation, especially in mountainous terrains.[3] In this study, we developed a relative displacement monitoring instrument using the microcomputer Raspberry Pi, a high-quality (HQ) camera module, telescopic lens, and chessboard. A computer-vision-based displacement monitoring (CVDM) system includes the instrument and user interfaces with the computer vision technology of the OpenCV library and Python programming. Moreover, we use solar power and the 5G network for 24 h slope monitoring in the CVDM system.

In recent years, computer vision technology has been used to evaluate construction safety using information obtained from images and videos.[4,5] There are also some applications of image recognition technology and IoT transmission to the displacement data detected in flood or landslide disasters.[6,7] However, image and video data used in previous studies, such as AI-trained aerial images or stereo image pairs, were not well suited for displacement detection over long distances or continuous 24 h monitoring.

In this study, we focus on innovative instruments for the long-distance and long-term monitoring of displacement detection using computer vision technology. The precision of the instruments can be comparable to that of traditional surveying instruments such as theodolites. The system of the instruments is designed to be a real-time, solar-powered, noncontact, cost-effective, and artificial intelligence of things (AIoT)-based system for displacement monitoring on a slope.

2. Materials and Methods

The CVDM instrument is applied to three-dimensional displacement measurements for civil engineering structures. The principle is similar to theodolite measurements, where a chessboard is set at a potential moving point, and the CVDM instrument is installed at a relatively fixed point. The computer vision technology analyzes image changes of the chessboard caused by relative displacements between the fixed and moving points, as shown in Fig. 1. When there is a relative displacement between the moving (chessboard) and fixed (CVDM instrument) points, the image of the chessboard captured by the camera of the CVDM instrument will also change. The CVDM system can calculate the changes in the pixels of the chessboard image to determine the amount of displacement using OpenCV library and Python programming.

The CVDM system uses the projection technology of camera images, as shown in Fig. 2.[8,9] A point Q in real-world coordinates (X, Y, Z) is projected onto the image plane through a ray passing through the camera projection center, and the resulting point on the image is $q = (x, y, f)$ in Fig. 2(a), where x and y indicate the imaging plane coordinates and f means the focal length of the lens.

$$x_{screen} = f_x\left(\frac{X}{Z}\right) + c_x \quad \text{and} \quad y_{screen} = f_y\left(\frac{Y}{Z}\right) + c_y \tag{1}$$

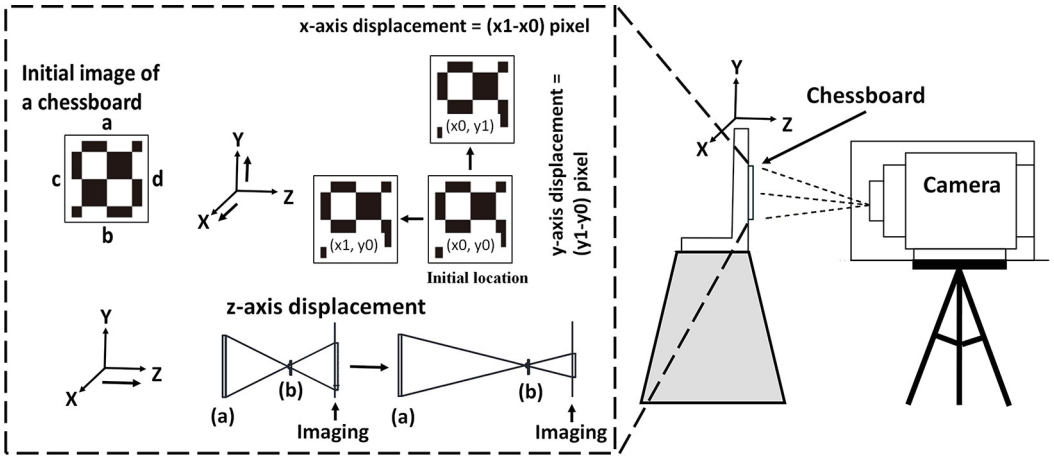

Fig. 1. Principle of CVDM instrument.

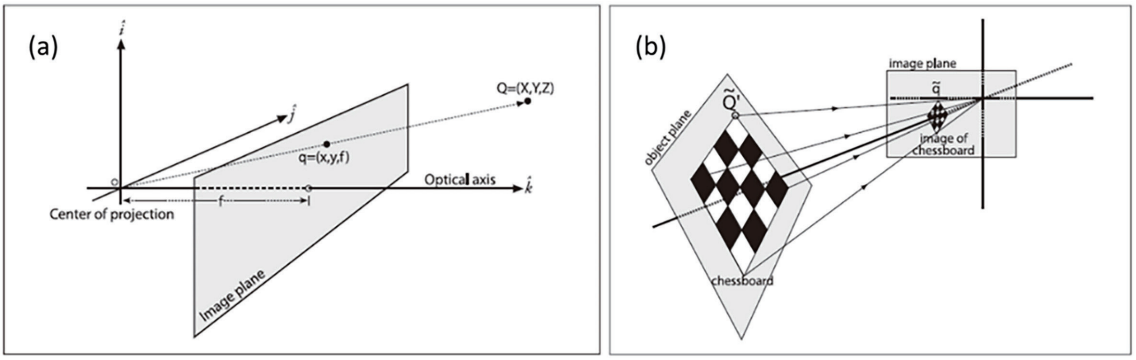

Fig. 2. Principle of computer-vision-based image recognition.[8]

Then, the parameters f_x, f_y, c_x, and c_y of the camera can be rearranged into a 3 × 3 matrix, known as the camera intrinsic matrix.[8,9] The projection of the points in the physical world into the camera is summarized as

$$\vec{\boldsymbol{q}} = \boldsymbol{M} \cdot \vec{\boldsymbol{Q}}, \text{ where: } \vec{\boldsymbol{q}} = \begin{bmatrix} x \\ y \\ w \end{bmatrix}, \ \boldsymbol{M} = \begin{bmatrix} f_x & 0 & c_x \\ 0 & f_y & c_y \\ 0 & 0 & 0 \end{bmatrix}, \text{ and } \vec{\boldsymbol{Q}} = \begin{bmatrix} X \\ Y \\ Z \end{bmatrix}. \tag{2}$$

Next, planar homography was defined as projective mapping from one plane to another, as shown in Fig. 2(b).[8] A mapping from the object plane to the image plane simultaneously comprehends the relative locations of those two planes as well as the camera projection matrix using

$$\vec{q} = s \cdot \boldsymbol{M} \cdot \boldsymbol{W} \cdot \vec{\boldsymbol{Q}}, \tag{3}$$

where s is an arbitrary scale factor and $\boldsymbol{W} = |\boldsymbol{R}\vec{\boldsymbol{t}}|$, with $\boldsymbol{R}$ being the rotation matrix and $\vec{\boldsymbol{t}}$ the translation matrix.

In this study, we use OpenCV library (cvCalibrateCamera2 and cvFindChessboardCorners) to automatically record the coordinates of the chessboard image that is calculated using its center positions and perimeter.[10,11] Changes in distance between the camera and the chessboard can be detected, as both the camera focal length and the chessboard dimensions are known. The relative displacement of the chessboard center point is calculated using Eq. (4). Thus, the actual displacement per unit pixel in the X- and Y-directions of the center point is determined.

$$\frac{Actual\ length\ of\ the\ chessboard\ (\text{cm})}{Image\ length\ of\ the\ chessboard\ (\text{pixels})} = Relative\ length\ (\text{cm})\ \ per\ pixel \tag{4}$$

The actual distance (d) between the lens and the target for the Z-direction is calculated using the focal length of the camera (f) and scale using Eq. (5), where W means the actual side length of the chessboard (cm), w means the image of the side length (pixels), and d means the distance between the lens and the chessboard.

$$d = \frac{f \times W}{w} \tag{5}$$

The experimental configuration of the CVDM system used in this study is illustrated in Fig. 3. The CVDM instrument comprises the microcomputer Raspberry Pi 4B, an HQ camera module, industrial and telescope lenses, and a chessboard.

The experimental tests for the CVDM instrument were conducted using two different lenses. One was an industrial lens mounted on the HQ camera module for the fixed-point observation at a short distance of 50 cm. The second setup employed a telescopic lens mounted on the HQ camera module at an extended range of 50 m. Specifications of the CVDM devices are shown in Table 1. Moreover, we developed an innovative solar-powered cubic chessboard integrated with LED lights. The LED cubic chessboard consists of six acrylic chessboard sheets (20 × 20 cm each), six solar panel modules, and two low-power LED lights, specifically designed to enable continuous 24-h monitoring for long-distance displacement measurements under nighttime conditions.

2.1 CVDM testing using an industrial lens

A 20-cm-square chessboard was set up on a manually adjustable stage platform for the static observation at a distance of 50 cm, as shown in Fig. 3. Pixels in the X-, Y-, and Z-directions of the chessboard were collected under the static condition using OpenCV Python programming. Then, the average value and standard deviation in accuracy test results were determined and are

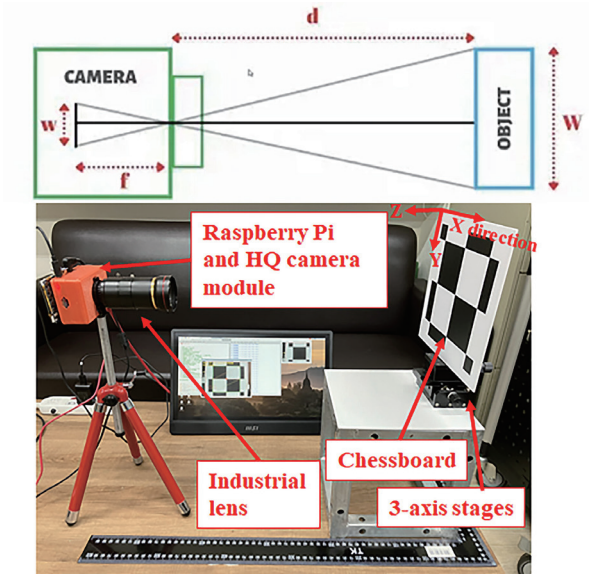

Fig. 3. (Color online) Configuration of CVDM system.

Table 1
Specifications of CVDM devices.

Raspberry Pi 4B	BCM2711, ARM Cortex-A72, 8 GB of RAM
HQ camera module	Raspberry Pi HQ Camera Sony IMX477R stacked sensor, 1/2.3", 12.3 megapixels
Industrial lens	Zoom lens, focal length: 12–120 (mm), resolution: 300 megapixels
Telescope	Focal length: 500 (mm), Optical tube: 80 (mm), 45–60× magnification
Cubic LED chessboard	Size of chessboard: 20 × 20 cm^2, 6 sets of 1.5 W solar panels, 2 sets of 2 W LEDs

shown in Table 2. The average values of the image center and perimeter of the chessboard in the *X*-, *Y*-, and *Z*-directions were 390.221, 285.882, and 174.417 pixels, respectively. The standard deviations in the *X*-, *Y*-, and *Z*-directions were 0.05, 0.04, and 0.06 pixels, respectively, for a total of 2574 data numbers during 10 min. Additionally, most of the observed data fell within two standard deviations.

Furthermore, 3-axis stages with the chessboard were moved 1 cm in the *X*-, *Y*-, and *Z*-axes. The movement of the chessboard was detected as the change in pixels of its image using the CVDM system. The error in the testing results was analyzed and is shown in Table 3. The average error in the *X*-, *Y*-, and *Z*-directions is 0.01 cm for a total of 2574 data numbers per direction. The error is the same as that of a traditional theodolite.

2.2 CVDM testing using a telescope lens

The CVDM instrument equipped with a telescopic lens was employed to detect a solar-powered cubic chessboard integrated with LED lights, with which ultralong-distance, continuous 24 h monitoring was possible. The solar panels were embedded on the surface of the chessboard to become part of black zones in the chessboard, as shown in Fig. 4(a).

Table 2
Indoor accuracy test results of fixed-point observation in CVDM using an industrial lens.

	X-axis direction	*Y*-axis direction	*Z*-axis direction
Average (pixel)	390.221	285.882	174.417
Standard deviation (pixel)	0.058	0.042	0.067
Amount of data (number)	2574	2574	2574
Twice the standard deviation (%)	98.25	96.19	97.75

Note: One pixel represents a length of 0.16 cm

Table 3
Indoor error test results in CVDM using an industrial lens.

Moving direction	Actual movement (cm)	Displacement measured by instrument (cm)	Error (cm)	Amount of data
X-axis	1	−0.9907	0.0092	2574
Y-axis	1	−0.9954	0.0046	2574
Z-axis	1	1.0107	0.0107	2574

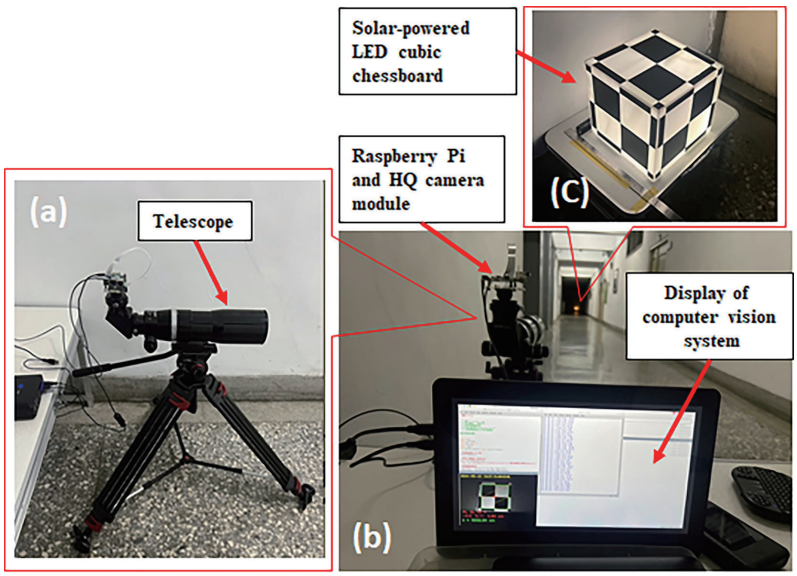

Fig. 4. (Color online) Configuration of indoor CVDM system with a telescope. (a) Set of Raspberry Pi, HQ camera, and telescope lens. (b) CVDM devices and display. (c) Solar-powered LED cubic chessboard.

In the long-distance testing, as shown in Fig. 4(b), the CVDM system was set up to statically detect the LED cubic chessboard for 72 h at a distance of 50 m in the experimental test. Then, the average value and standard deviation of the testing results were analyzed and are shown in Table 4. The average values of the image center and perimeter of the chessboard in the *X*-, *Y*-, and *Z*-directions were 466.145, 217.359, and 231.447 pixels, respectively, with an average standard deviation of 0.955 pixels. Given that a pixel represents 0.105 cm at 50 m in the test, the average precision is 0.100 cm.

Table 4
Indoor accuracy test of 50 m distance for CVDM with a telescope lens.

	X-axis direction	*Y*-axis direction	*Z*-axis direction
Average (pixel)	466.145	217.359	231.447
Standard deviation (pixel)	1.469	0.686	0.709
Amount of data (number)	668971	668971	668971
Amount of twice the standard deviation (%)	98.50	97.07	95.73

Note: One pixel represents a length of 0.105 cm.

3. Field Testing

3.1 CVDM with a telescope lens in 1000-m-distance measurement

The experimental method in the 1000-m-distance measurement was similar to that in the previously conducted 50 m indoor experiment; however, a larger chessboard size (85 × 85 cm^2) was employed to facilitate measurements at long distances exceeding 1000 m along a river embankment. Figure 5(a) shows that a larger chessboard with a size of 85 × 85 cm^2 was installed on the river embankment because a smaller chessboard cannot be detected in image recognition using the computer vision programming. A theodolite was set up beside the CVDM instrument, as shown in Fig. 5(b), to measure the initial reference distance. A retroreflective surveying prism was placed beside the chessboard, and the measured distance of 100487 cm between the theodolite and the prism was entered as a parameter into the CVDM programming for calculating the changes in *X*-, *Y*-, and *Z*-axis image pixels. Figure 5(d) shows the display of the computer vision program within the CVDM system, illustrating the detection of the chessboard.

To evaluate the effect of a high image resolution on the measurement accuracy of the CVDM instrument under ultralong-distance conditions, two different image resolutions (1280 × 960 and 1920 × 1440 pixels) were tested. Static measurement errors along the X-, Y-, and Z-axes were recorded during a designated field testing period. The monitoring results for each resolution are presented in Fig. 6.

The image resolutions of 1280 × 960 and 1920 × 1440 pixels represent actual lengths of 0.83 and 0.56 cm per pixel, respectively, in the CVDM system in the field. The standard deviations of average *X*-, *Y*-, and *Z*-axis image recognition accuracies in the chessboard for the image resolutions of 1280 × 960 and 1920 × 1440 were 0.33 and 0.39 pixels, corresponding to actual displacements of 0.27 and 0.22 cm, respectively, as shown in Table 5. Nevertheless, the amount of data in the image with a resolution of 1280 × 960 is 2400 sets during 10 min, which is more than the 600 sets in the case of 1920 × 1440 resolution. Thus, the image resolution of 1280 × 960 is suitable for the CVDM setup in the long-distance test. The results show that the recognition and precision for the distance of more than 1000 m are acceptable for the CVDM system.

3.2 Long-term displacement monitoring for a landslide slope

The CVDM system was installed in the Jiufenershan landslide area in Nantou County as a case study. The area of the Jiufenershan landslide is 195 hectares within which severe landslides

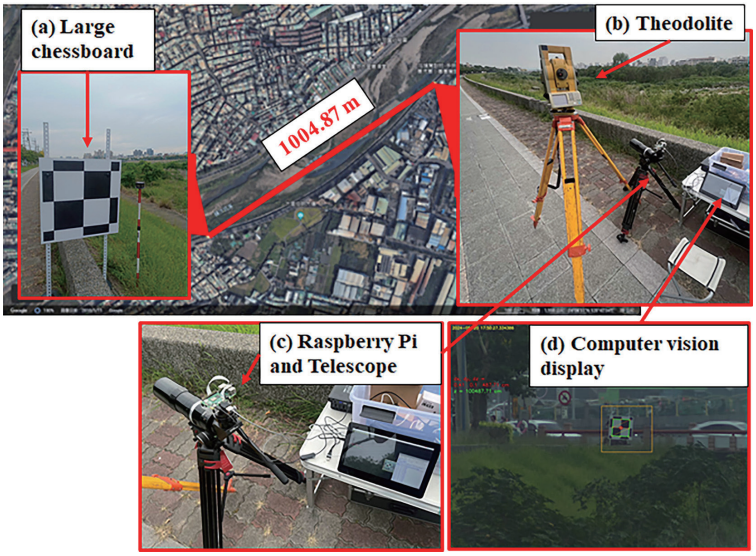

Fig. 5. (Color online) Setup of CVDM using a telescope lens for observation over a long distance exceeding 1000 m.

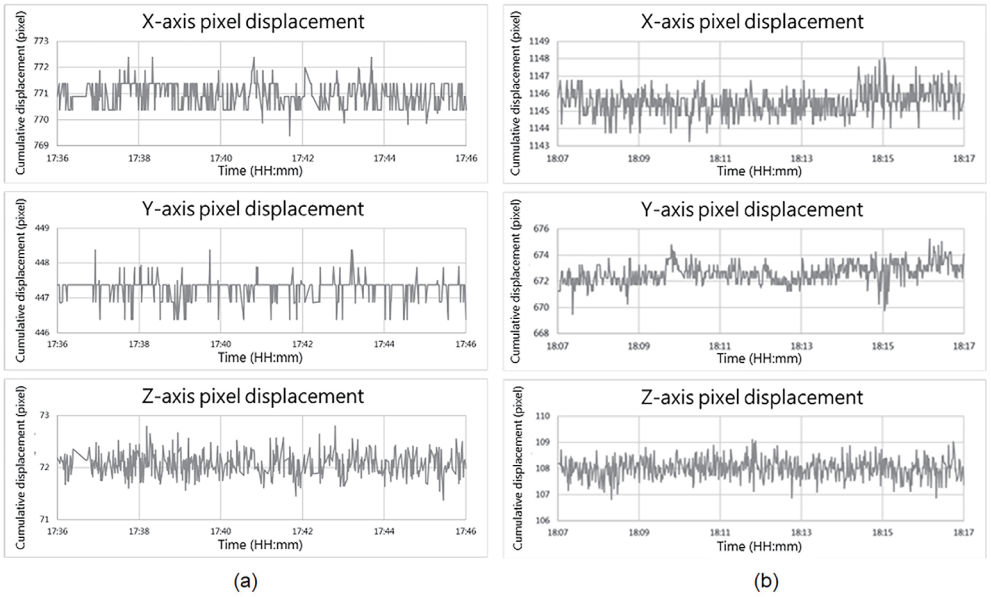

Fig. 6. Monitoring graphs of CVDM system for 1000-m-distance measurement. Image resolutions of (a) 1280 × 960 pixels and (b) 1920 × 1440 pixels.

Table 5
Accuracy test results of CVDM with a telescope lens for a measurement distance of more than 1000 m.

		X-axis direction	*Y*-axis direction	*Z*-axis direction	Average
Image resolution	Amount of data (number)	Standard deviation (Pixel)			
1280 × 960 (0.83 cm per pixel)	717	0.38	0.32	0.22	0.33
1920 × 1440 (0.56 cm per pixel)	615	0.39	0.39	0.38	0.39

occurred accompanying the 1999 Chi-Chi earthquake. The amount of collapse in the event was 35 million cubic meters. Remediation works and vegetation restoration projects have been undertaken in the area. However, the area remains a dangerous zone for landslides.[12]

The CVDM instrument and a solar-powered LED cubic chessboard were set up on both sides of the Longnan Road in the landslide area. The distance between the CVDM instrument and the LED chessboard was 33 m. The instrument was placed in a monitoring enclosure with a height of 200 cm, a length of 60 cm, and a width of 50 cm with a solar power of 100 W for 24 h monitoring, as shown in Fig. 7.

The LED cubic chessboard was placed on the landslide slope. Then, the CVDM system continuously measured the relative displacement of the chessboard in real time. The monitoring data and chessboard images were simultaneously transmitted to a cloud database through a 5G IoT network.

First, analytic results of data from the 24 h real-time CVDM are shown in Table 6. The average pixel values of the detected target image center and edge pixels in the *X*-, *Y*-, and *Z*-directions were 536.31, 268.68, and 338.53, respectively. There were 568503 sets of one-day monitoring data per axis in the CVDM system. The standard deviations in the *X*-, *Y*-, and

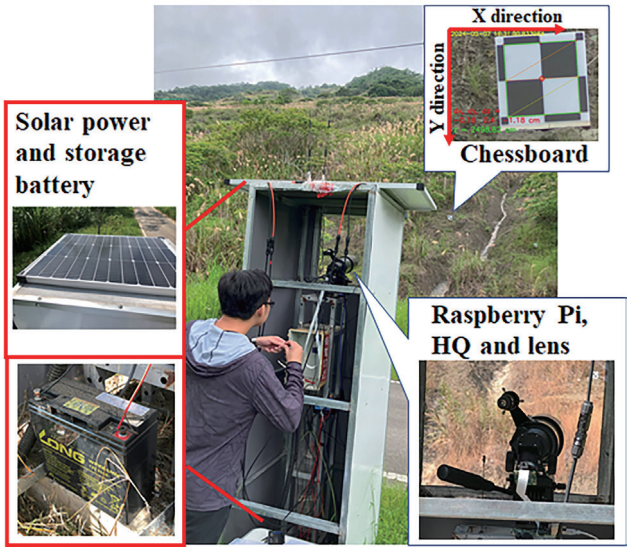

Fig. 7. (Color online) On-site configuration of CVDM instrument and chessboard on landslide slope.

Table 6
Accuracy test results of 33-m-distance measurement using CVDM in Jiufenershan area.

	X-axis direction	*Y*-axis direction	*Z*-axis direction
Average (pixel)	536.31	268.68	338.53
Standard deviation (pixel)	1.53	3.36	2.64
Amount of data (number)	568503	568503	568503
Amount of twice the standard deviation (%)	97.69	99.45	96.54

Note: One pixel represents a length of 0.089 cm.

Z-directions were 1.53, 3.36, and 2.64 pixels, respectively. One pixel represented a length of 0.089 cm in the case study, so the average precision was 0.22 cm.

Second, the long-term monitoring data from December 23 to 30, 2024 are shown in Fig. 8. Figure 8(a) shows that temperature changes caused monitoring data fluctuations between −0.5 and 0.5 cm in the *X*-displacement direction but the changes remained within a millimeter-level error. The on-site CVDM system was effective for monitoring during rainy weather both in the daytime and at night from Dec. 23 to 24 in the landslide area, as shown in Fig. 8(b). There was a settlement of *Y* displacement by approximately 1 cm in the evening of Dec 28. Consequently, the CVDM can be set up to detect ground movement for 24 h real-time monitoring on the slope. In the case study, the average precision and error of CVDM were 0.22 and 0.5 cm, respectively. Overall, the effect of temperature on the slope displacement measurements was found to be negligible. Although rainfall may induce temperature fluctuations and potentially affect slope

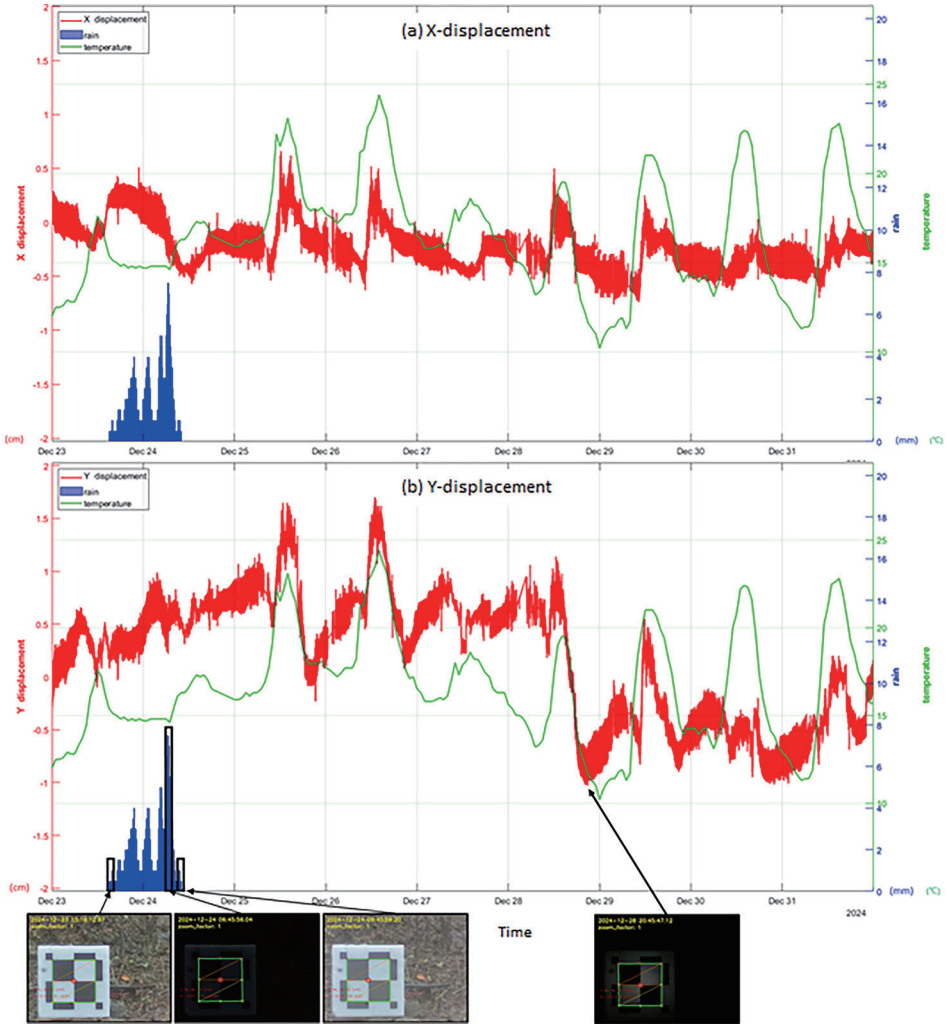

Fig. 8. (Color online) Relationship between *X*- and *Y*-axis displacements, precipitation, and temperature for seven days of single-lens fixed-point observation test in Jiufenershan landslide area.

displacements, no significant effects were observed during the monitoring periods shown in Fig. 8.

3.3 AIoT application

Monitoring data and images of the CVEM system are transmitted to a cloud database via 5G in this study. The CVDM system detects the *XYZ* three-direction displacement of the LED cubic chessboard on the landslide slope. Moreover, the system displays real-time monitoring data in accordance with the IoT flow chart shown in Fig. 9. To ensure 24 h operation, the Raspberry Pi of the CVMD automatically reboots daily to clear its cache and run image recognition programs with Python programming. Then, monitoring data from records of *XYZ* displacements, including pixel values of the center point and perimeter edge of the chessboard and pixel-to-centimeter conversion format, are stored in JSON format. Furthermore, the image data were recorded at an average rate of 4 frames per second using OpenCV programming, with the data transmitted to the cloud server at 10 min intervals. Finally, the AIoT application is capable of displaying synchronized multidimensional monitoring data and images on a web-based platform, as shown in Fig. 10. The displayed information includes the original pixel values in the *X*-, *Y*-, and *Z*-directions, the corresponding converted displacement values in centimeters, and the on-site images of the chessboard.

4. Discussion

In this study, we developed a three-axis displacement-detecting instrument embedded in a telescope for long-distance measurement using computer vision technology. Figure 10 illustrates the design drawing of the CVDM instrument, which includes the Raspberry Pi recording module with a camera embedded in a telescope, and a solar-powered LED chessboard that can be monitored 24 h a day, both during the day and at night.

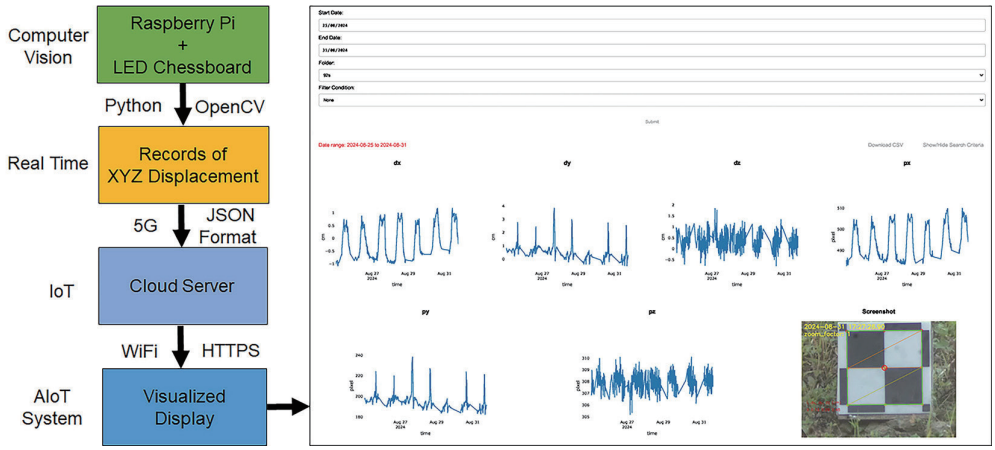

Fig. 9. (Color online) Flowchart and display of AIoT system and data for CVDM instrument.

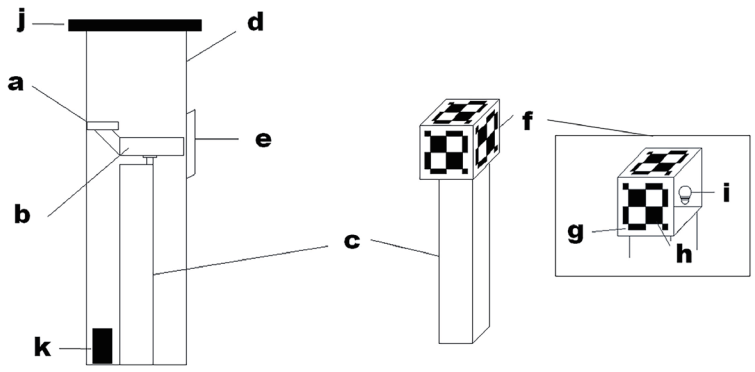

Fig. 10. Design drawing of CVDM instrument: (a) Raspberry Pi and HQ camera, (b) telescope, (c) steel frame, (d) stainless-steel enclosure, (e) window of enclosure, (f) LED chessboard, (g) translucent material checkerboard, (h) small solar panel, (i) LED, (j) large solar panel, and (k) storage battery.

Computer-vision-based approaches are gaining increasing attention in the field of geotechnics because of their advantages such as noncontact, real-time, and low-cost operation.[13,14] However, there are some limitations of computer vision including heavy rain, lighting at night, and camera distance.[15,16] This is why it is important to continually develop a telescope embedded in the CVDM system for long distances and solar-powered lights embedded in the chessboard for 24 h monitoring, as shown in Figs. 10(b) and 10(f). On the other hand, we designed a stainless-steel enclosure where the CVDM instrument is installed so as to stably detect the displacement of the chessboard against adverse environmental conditions (rain, water, and wind), as shown in Fig. 10(d). The use of computer-vision- and IoT-based sensors is proposed to make the wireless and solar-powered system more energy efficient.[17–19] Thus, one set of 100 W solar power and four sets of 240 Wh storage batteries were used for 24 h monitoring in this study, as shown in Figs. 10(j) and 10(k), respectively. Moreover, small solar panels and a rechargeable battery were incorporated in the LED chessboard, as shown in Figs. 10(h) and 10(i).

Finally, the microcomputer Raspberry Pi and a 5G dongle integrated within the CVDM instrument are shown in Fig. 10(a), and the solar-powered LED chessboards are mounted on an iron rack [Fig. 10(c)]. The CVDM instrument detects relative displacements of the chessboard in real time and transmits both the monitoring data and images to a cloud database via 5G IoT connectivity, forming a novel AIoT-based monitoring system.

The on-site CVDM instrument with the Raspberry Pi, a telescopic lens, chessboard, solar-powered system, and stainless-steel enclosure costs about USD 2,000, so it is a cost-effective solution at roughly one-fifth the cost of conventional instruments such as total stations or GNSS systems. Moreover, the CVDM system provides a measurement precision of up to 0.01 cm with the advantages of power efficiency, 24 h monitoring, and IoT-based application of data and images. Table 7 shows that the cost of a CVDM instrument is much less than those of traditional monitoring devices, and its resolution is better than that of the GNSS. In addition, the CVDM is an IoT system with computer vision technology and 5G wireless communication.

Table 7
Characteristics of CVDM instrument and traditional monitoring devices.

	CVDM	Total station	GNSS
Resolution	0.01 cm	0.01–0.1 cm	0.1–2 cm
Price	$2000 USD	$10000–15000 USD	$6000–10000 USD
IoT application	Yes	No	Yes, if connected to other devices.[20]

Up to now, many computer-vision-based approaches have been applied to the measurement of structures such as bridges, retaining walls, and tunnels.[21] However, these on-site measuring distances were between 1 and 50 m. Longer distances are often required for the measurement of structures such as embankments, landslide slopes, and dams, whereas the instruments of the above approaches were limited and the measurement accuracy decreased with increasing measurement distance. We devised a new instrument for displacement measurement to detect ultralong distances of 1000 m along a river embankment using a microcomputer, telescope, and computer vision technology. An optical- or computer-vision-based instrument is often affected by the environmental temperature and light, which causes fluctuations of monitoring data.[22,23] Thus, a stainless-steel enclosure was designed to house the CVDM instrument, minimizing environmental effects such as dust, rain, and wind fluctuations. We also developed a solar-powered LED chessboard comprising small solar panels and a rechargeable battery, effectively addressing the illumination challenges during nighttime monitoring. The results of long-term field monitoring indicate that the CVDM system achieves an average error of approximately 0.5 cm for a 24 h real-time monitoring system. Consequently, the CVDM instrument will be applicable to the monitoring of longer distance for bridges, dams, buildings, and offshore wind turbine foundations in the future.

5. Conclusions

In this study, we developed an innovative sensor for ground movement monitoring for ultralong-distance and long-term measurement using computer vision technology. The solar-powered LED cubic chessboard measuring target was designed to solve light problems during nighttime measurement. The CVDM instrument was shown to be a 24 h, real-time, energy-saving, cost-effective, and AIoT-based device for slope monitoring. The resolution of the *XYZ*-direction displacements in the CVDM instrument was 0.01 cm. The average precisions of displacement measurements in the *X*-, *Y*-, and *Z*-directions using the CVDM instrument were 0.10 cm at a distance of 50 m in indoor tests, 0.22 cm at a distance of 33 m on a landslide slope, and 0.27 cm at a distance of 1000 m along a river embankment.

The CVDM instrument was deployed on a landslide slope to detect the displacement of the solar-powered LED cubic chessboard through 24 h, real-time, IoT-based monitoring. Although the long-term monitoring data showed fluctuations in the displacements owing to temperature changes, average errors for the *XYZ*-direction displacements were less than 1 cm. The on-site CVDM system proved to be an effective monitoring device capable of operating continuously under rainy weather conditions in a landslide area. The CVDM system achieved a real-time image recognition rate averaging four frames per second, with monitoring data and images

being transmitted to a cloud database via 5G at 10 min intervals in this study. In the future, the innovative CVDM instrument should be able to provide noncontact, ultralong-distance, and cost-effective displacement monitoring for the monitoring of engineering structures. The fluctuations and decreases in errors of the data from CVDM will be postprocessed using moving average or Gaussian filter methods.

Acknowledgments

This research was supported by the Agency of Rural Development and Soil and Water Conservation (ARDSWC), MOA, Taiwan. This research is part of one of the Innovative Research Projects in ARDSWC. The main objective of the Innovative Research Projects is to build a core center with forward-looking strategies, techniques, and data for disaster prevention in Taiwan.

References

1 R. Ray and M. Lazzari (Eds.): Landslides - Investigation and Monitoring (IntechOpen, 2020). https://doi.org/10.5772/intechopen.78130
2 M. B. Su, I. H. Chen, and C. H. Liao: J. Geotech. Geoenviron. Eng. **135** (2009) 1113. https://doi.org/10.1061/(ASCE)GT.1943-5606.0000074
3 R. E. Hunt: Geotechnical investigation methods: a field guide for geotechnical engineers (CRC/Taylor & Francis, Boca Raton, 2007).
4 T. Khuc and F. N. Catbas: Struct. Infrastruct. Eng. **13** (2017) 505. https://doi.org/10.1080/15732479.2016.1164729
5 H. Luo, C. Xiong, W. Fang, P. E. Love, B. Zhang, and X. Ouyang: Autom. Constr. **94** (2018) 282. https://doi.org/10.1016/j.autcon.2018.06.007
6 I. H. Chen, S. C. Ho, and M. B. Su: Autom. Constr. **110** (2020) 103011. https://doi.org/10.1016/j.autcon.2019.103011
7 Y. C. Chen, I. H. Chen, J. Y. Chen, and M. B. Su: Sens. Mater. **33** (2021) 995. https://doi.org/10.18494/SAM.2021.3011
8 G. Bradskia and A. Kaehler: Learning OpenCV: Computer Vision with the OpenCV Library (O'Reilly Media, Inc., California, 2008).
9 A. Khongma, M. Ruchanurucks, T. Koanantakool, T. Phatrapornnant, Y. Koike, and P. Rakprayoon: Kinect Quality Enhancement for Triangular Mesh Reconstruction with a Medical Image Application (Springer, Cham, 2014) p. 15. https://doi.org/10.1007/978-3-319-04693-8_2
10 OpenCV modules: https://docs.opencv.org/4.9.0/ (accessed December 2023).
11 Open Source Computer Vision Library: https://github.com/opencv/opencv/tree/4.9.0 (accessed December 2023).
12 S. C. Ho, I. H. Chen, Y. S. Lin, J. Y. Chen, and M. B. Su: Landslides **16** (2019) 1141. https://doi.org/10.1007/s10346-019-01139-1
13 C. Z. Dong, S. Bas, and F. N. Catbas: Smart Struct. Syst. **24** (2019) 617. https://doi.org/10.12989/sss.2019.24.5.617
14 B. Bučko, E. Lieskovská, K. Zábovská, and M. Zábovský: Sensors **22** (2022) 8878. https://doi.org/10.3390/s22228878
15 D. Ai, G. Jiang, S. K. Lam, P. He, and C. Li: Eng. Appl. Artif. Intell. **117** (2023) 105478. https://doi.org/10.1016/j.engappai.2022.105478
16 B. Arshad, R. Ogie, J. Barthelemy, B. Pradhan, N. Verstaevel, and P. Perez: Sensors **19** (2019) 5012. https://doi.org/10.3390/s19225012
17 C. Moreno, R. Aquino, J. Ibarreche, I. Pérez, E. Castellanos, E. Álvarez, R. Rentería, L. Anguiano, A. Edwards, and P. Lepper: Sensors **19** (2019) 127. https://doi.org/10.3390/s19010127
18 I. H. Chen, Y. S. Lin, and M. B. Su: Landslides **17** (2020) 1009. https://doi.org/10.1007/s10346-019-01329-x
19 O. R. Jan, H. S. Jo, R. S. Jo, and J. Kua: Future Internet **14** (2022) 308. https://doi.org/10.3390/fi14110308

20 D. Egea-Roca, M. Arizabaleta-Diez, T. Pany, Antreich, F, J. Lopez-Salcedo, M. Paonni, and G. Seco-Granados: GNSS user technology: State-of-the-art and future trends (IEEE Access, 10, 2022) 39939.
21 Y. Zhuang, W. Chen, T. Jin, B. Chen, H. Zhang, and W. Zhang: Sensors **22** (2022) 3789. https://doi.org/10.3390/s22103789
22 B. Ko and S. Kwak: Opt. Eng. **51** (2012) 070901. https://doi.org/10.1117/1.OE.51.7.070901
23 M. R. Ibrahim, J. Haworth, and T. Cheng: ISPRS Int. J. Geo-Inf. **8** (2019) 549. https://doi.org/10.3390/ijgi8120549